Evolution of the pygmy dipole resonance in Sn isotopes

H. K. Toft,[1,*] A. C. Larsen,[1] A. Bürger,[1] M. Guttormsen,[1] A. Görgen,[1] H. T. Nyhus,[1] T. Renstrøm,[1] S. Siem,[1] G. M. Tveten,[1] and A. Voinov[2]

[1]*Department of Physics, University of Oslo, N-0316 Oslo, Norway*

[2]*Department of Physics and Astronomy, Ohio University, Athens, Ohio 45701, USA*

(Received 26 November 2010; revised manuscript received 9 February 2011; published 25 April 2011)

Nuclear level density and γ-ray strength functions of ^{121,122}Sn below the neutron separation energy are extracted with the Oslo method using the (^{3}He,^{3}He$'\gamma$) and (^{3}He,$\alpha\gamma$) reactions. The level densities of ^{121,122}Sn display steplike structures, interpreted as signatures of neutron pair breaking. An enhancement in both strength functions, compared to standard models for radiative strength, is observed in our measurements for $E_\gamma \gtrsim 5.2$ MeV. This enhancement is compatible with pygmy resonances centered at $\approx$8.4(1) and $\approx$8.6(2) MeV, respectively, and with integrated strengths corresponding to $\approx 1.8^{+1}_{-5}$% of the classical Thomas-Reiche-Kuhn sum rule. Similar resonances were also seen in $^{116-119}$Sn. Experimental neutron-capture cross reactions are well reproduced by our pygmy resonance predictions, while standard strength models are less successful. The evolution as a function of neutron number of the pygmy resonance in $^{116-122}$Sn is described as a clear increase of centroid energy from 8.0(1) to 8.6(2) MeV, but with no observable difference in integrated strengths.

DOI: 10.1103/PhysRevC.83.044320 PACS number(s): 21.10.Ma, 24.10.Pa, 24.30.Gd, 27.60.+j

I. INTRODUCTION

The level density and the γ-ray strength function are average quantities describing properties of atomic nuclei. The nuclear level density is defined as the number of energy levels per unit of excitation energy, while the γ-ray strength function may be defined as the reduced average transition probability as a function of γ-ray energy. The strength function characterizes average electromagnetic properties of excited nuclei.

The level density and the strength function are important for many aspects of fundamental and applied nuclear physics. They are used for the calculation of cross sections and neutron-capture (n,γ) reaction rates, which are input parameters in, e.g., reactor physics, nuclear waste management, and astrophysical models describing the nucleosynthesis in stars.

Tin and other heavier neutron-rich nuclei are often found to display a smaller resonance for γ-ray energies below the giant electric dipole resonance (GEDR). The existence of even a small resonance close to the neutron separation energy may have large consequences in nuclear astrophysics on the calculated distribution of elemental abundance.

This paper presents the measurements of the level densities and γ-ray strength functions in ^{121,122}Sn for energies below the neutron separation energy, as well as a systematic study of the evolution of the pygmy resonances in $^{116\text{-}119,121,122}$Sn. The experimental results on $^{116\text{-}119}$Sn are published in Refs. [1–3]. All experiments have been performed at the Oslo Cyclotron Laboratory (OCL).

The experimental setup is described in Sec. II and the data analysis in Sec. III. The level densities of ^{121,122}Sn are presented in Sec. IV and the strength functions in Sec. V. Section VI discusses the pygmy resonance evolution and the impacts from the pygmy resonances on the (γ,n) cross sections. Conclusions are drawn in Sec. VII.

*h.k.toft@fys.uio.no

II. EXPERIMENTAL SETUP

The self-supporting ^{122}Sn target was enriched to 94% and had a mass thickness of 1.43 mg/cm^2. For five days the target was exposed to a 38 MeV ^{3}He beam with an average current of $\approx$0.2 nA. The reaction channels studied were ^{122}Sn(^{3}He,^{3}He$'\gamma$)^{122}Sn and ^{122}Sn(^{3}He,$\alpha\gamma$)^{121}Sn.

Particle-γ coincidences were recorded with 64 Si particle $\Delta E - E$ telescopes and 28 collimated NaI(Tl) γ-ray detectors. The ΔE and E detector thicknesses are approximately 130 and 1550 μm, respectively. These detectors cover the angles of 40°-54° with respect to the beam axis, and they have a total solid-angle coverage of $\approx$9% out of 4π. The NaI detectors are distributed on a sphere and constitute the CACTUS multidetector system [4]. The detection efficiency is 15.2%, and the resolution of a single NaI detector is $\approx$6% FWHM, at the γ energy of 1332 keV.

III. DATA ANALYSIS

The measured energy of the ejectile is calculated into excitation energy of the residual nucleus. The γ-ray spectra are unfolded with the known response functions of CACTUS and by the use of the Compton subtraction method [5]. The first generation γ-ray spectra are extracted by the subtraction procedure described in Ref. [6].

The first-generation γ-ray spectra are arranged in a two-dimensional matrix $P(E, E_\gamma)$, shown for ^{122}Sn in Fig. 1. The entries of the matrix give the probabilities $P(E, E_\gamma)$ that a γ-ray of energy E_γ is emitted from a bin of excitation energy E.

The empty region for low γ energy and higher excitation energies in Fig. 1 is explained by too strong subtraction caused by the strongly populated states (yellow/red spots) found for low γ energy and lower excitation energies. Too few first-generation γ's remain for low γ energy and higher excitation

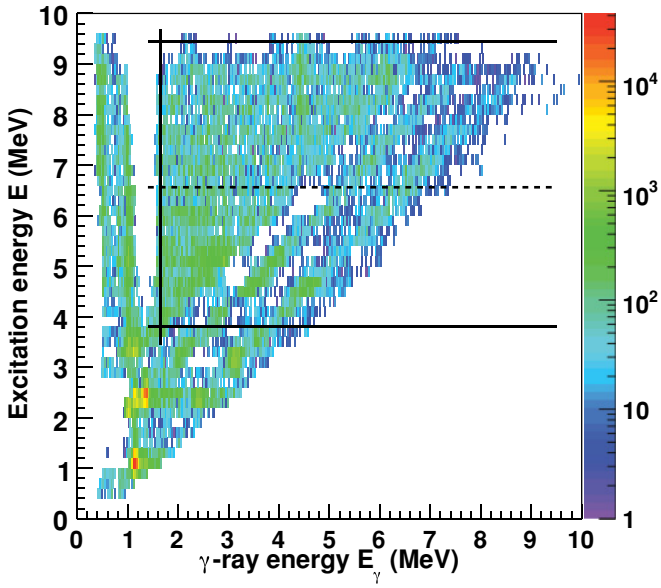

FIG. 1. (Color online) The first-generation matrix P of ^{122}Sn. The solid lines indicate the region for the data used in the Oslo method ($E_\gamma > 1.6$ MeV, $3.8 < E < 9.4$ MeV). The dashed line ($E = 6.6$ MeV) is the middle between the upper and lower ranges in excitation energy.

energies, which has made the first-generation method not work very well (see Ref. [7]). We select and proceed with the region between the solid lines. Note that the diagonal valleys and ridges are made up of strong first-generation transitions to the ground and first-excited states.

The selected region of the first-generation matrix P is factorized into the level density ρ and the radiative transmission coefficient $\mathcal{T}$ [8]:

$$P(E, E_\gamma) \propto \rho(E - E_\gamma)\mathcal{T}(E_\gamma). \quad (1)$$

The factorization into two independent components is justified for nuclear reactions leading to a compound state prior to a subsequent γ decay [9]. The factorization is performed by an iterative procedure [8] where the independent functions ρ and $\mathcal{T}$ are adjusted until a global χ^2 minimum with the experimental $P(E, E_\gamma)$ is reached.

The quality of the factorization of level density and strength function is illustrated for ^{122}Sn in Fig. 2. At example excitation energies (indicated on the panels), the entries of the P matrix obtained from the χ^2-fitted output functions ρ and $\mathcal{T}$ using Eq. (1) are compared to those of the experimental P matrix. The fitted output (solid line) agrees well with experimental data. It is noted that in some of the panels, the fitted curves are significantly lower than the experimental data points (for $E = 4.1$ MeV: the transition to the ground state; for $E = 4.8$ MeV: the transition to the first-excited state). This is probably explained by the fit adjusting the entire matrix, and not just these example excitation energies.

The Brink-Axel hypothesis [10,11] states that the GEDR and any other collective excitation mode built on excited states have the same properties as those built on the ground state. Equation (1) shows that the transmission coefficient is assumed to be independent of excitation energy E, which is a consequence of the Brink-Axel hypothesis.

Figure 3 shows an investigation of this assumption for ^{122}Sn, which is of special concern due to some clear structures

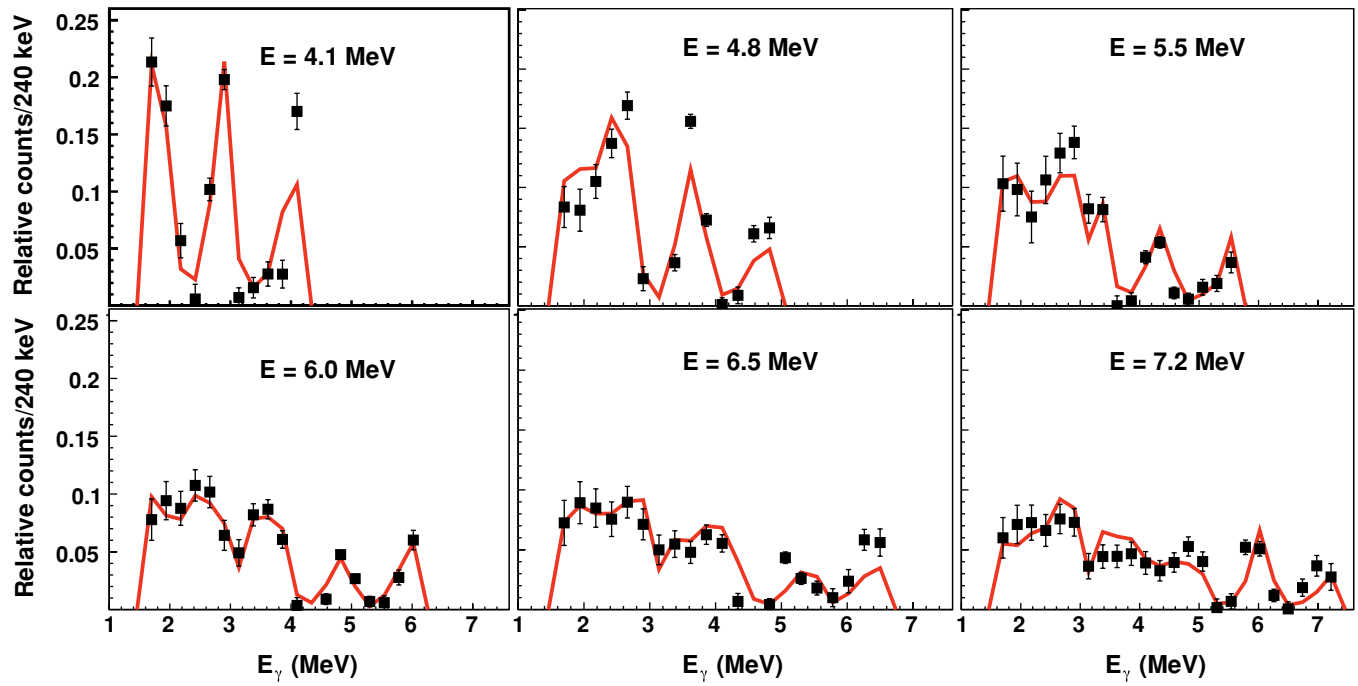

FIG. 2. (Color online) Comparison between experimental (squares) and χ^2 fitted (solid lines) P matrix for ^{122}Sn. The energy bins have been compressed to 240 keV/ch in E and E_γ. While the panels show the results for the indicated example excitation energies, the fit has been performed globally for the entire region of the P matrix that has been selected for the analysis (see Fig. 1).

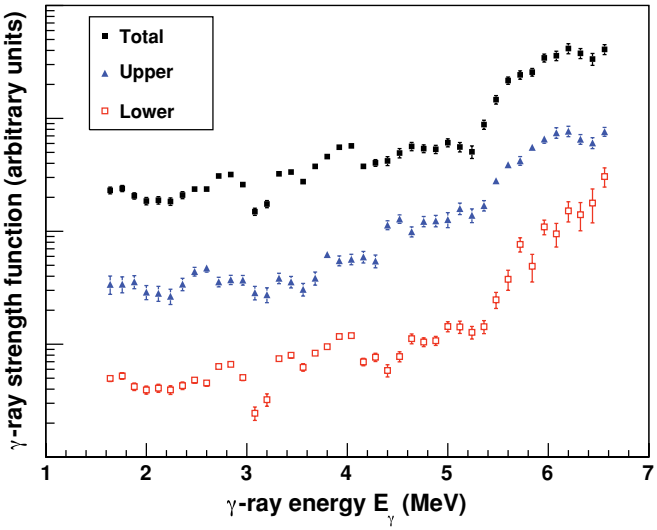

FIG. 3. (Color online) Comparison of unnormalized γ-ray strength functions (arbitrary units) for ^{122}Sn. The shown strength functions are derived from the independent data sets of the upper and lower parts of the selected region of the P matrix, as well as from the total selected region for comparison.

in the strength function. We divide the selected region of the P matrix into two parts (separated by the dashed line in Fig. 1), which are two independent data sets. Figure 3 displays the strength functions derived from the lower and upper parts, as well as from the total region. The strength functions, proportional to $\mathcal{T}/{E_\gamma}^3$, are not normalized and are shown in arbitrary units. As the clear structures are found at the same locations for the two independent data sets, the $\mathcal{T}$ is indeed found to be approximately independent of excitation energy.

The adjustment to Eq. (1) determines only the functional forms of ρ and $\mathcal{T}$. These two functions are invariant under the following transformations [8]:

$$\tilde{\rho}(E - E_\gamma) = A\ \exp[\alpha(E - E_\gamma)]\rho(E - E_\gamma), \quad (2)$$

$$\tilde{\mathcal{T}}(E_\gamma) = B\ \exp(\alpha E_\gamma)\mathcal{T}(E_\gamma). \quad (3)$$

The parameters A and B define the correction to the absolute values of the functions ρ and $\mathcal{T}$, respectively, while the parameter α defines their common correction to the log-scale slope. These parameters will be determined in Secs. IV and V.

IV. LEVEL DENSITIES

The constants A and α needed to normalize the experimental level density ρ, are determined using literature values of the known discrete energy levels at low energy and of the level spacing D at the neutron separation energy S_n. We use the same normalization procedure as in Refs. [1–3], in order to have a common ground for comparison.

The chosen model is the back-shifted Fermi-gas (BSFG) model, published by von Egidy *et al.* in 1988 [12]. The level density at the neutron separation energy $\rho(S_n)$ is calculated from known values of the s-wave level spacing D_0 [8]:

$$\rho(S_n) = \frac{2\sigma^2}{D_0}\left\{(I_t+1)\exp\left[\frac{-(I_t+1)^2}{2\sigma^2}\right] + I_t\ \exp\left[\frac{-{I_t}^2}{2\sigma^2}\right]\right\}^{-1}, \quad (4)$$

where I_t is the target spin, and where the spin-cutoff parameter σ is also evaluated at S_n. The spin-cutoff parameter is defined as $\sigma^2 = 0.0888A^{2/3}aT$, where A is the mass number of the isotope, and T is the nuclear temperature given by $T = \sqrt{U/a}$. Here, U is the nucleus intrinsic excitation energy and a is the level-density parameter. The parametrization used for a is $a = 0.21\ A^{0.87}$ MeV^{-1}. The parametrization of U is $U = E - E_{\text{pair}} - C_1$, where the pairing energy E_{pair} is calculated from the proton and neutron pair-gap parameters: $E_{\text{pair}} = \Delta_{\text{p}} + \Delta_{\text{n}}$, and where the back-shift parameter C_1 is defined as $C_1 = -6.6A^{-0.32}$.

The experimental value of D_0 for ^{121}Sn is found in Ref. [13] and is used to calculate $\rho(S_n)$ using the input parameters listed in Table I. The pair-gap parameters are evaluated from even-odd mass differences [14] according to the method of Ref. [15].

No experimental value exists for D_0 of ^{122}Sn, and we estimate $\rho(S_n)$ for this isotope from systematics. Figure 4 shows $\rho(S_n)$ calculated from the experimental values of D_0 according to Eq. (4) for all available Sn isotopes as a function of S_n. The values of D_0 have been taken from Ref. [13]. We have also calculated $\rho(S_n)$ according to the prediction of the BSFG model [16]:

$$\rho(E)_{\text{BSFG}} = \frac{\exp(2\sqrt{aU})}{12\sqrt{2}\,a^{1/4}\,U^{5/4}\,\sigma}, \quad (5)$$

with the above-listed parametrizations. The theoretical value of $\rho(S_n)$, multiplied with a common factor of 0.4, are shown in Fig. 4 together with the experimental values. From the trends appearing in the figure, we estimate $\rho(S_n)$

TABLE I. Input parameters and the resulting values for the calculation of the normalization value $\rho(S_n)$.

Nucleus	S_n (MeV)	D_0 (eV)	a (MeV^{-1})	C_1 (MeV)	Δ_{n} (MeV)	Δ_{p} (MeV)	$\sigma(S_n)$	$\rho(S_n)$ (10^4 MeV^{-1})	η
^{121}Sn	6.17	1250(200)	13.62	−1.42	0	0.82	4.57	3.42(86)	0.25
^{122}Sn	8.81	62(31)[a]	13.72	−1.42	1.32	1.12	4.75	20(10)[a]	0.42

[a]Estimated from systematics.

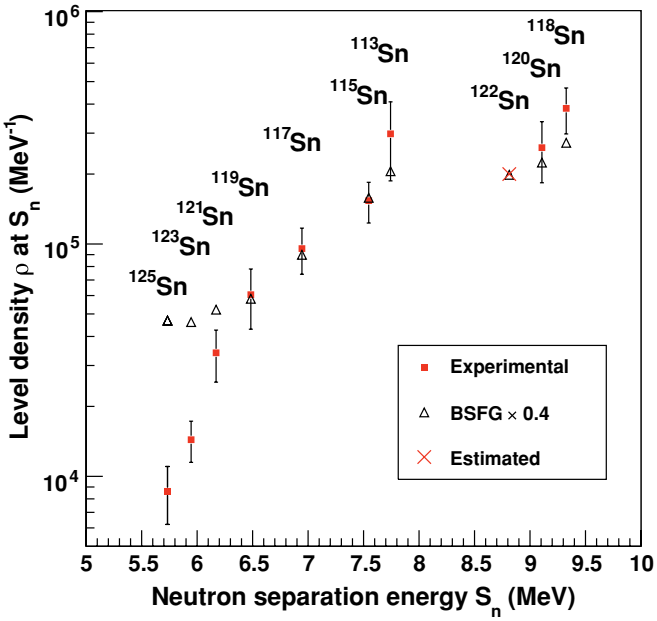

FIG. 4. (Color online) Estimation (cross) of the experimental value of $\rho(S_n)$ for ^{122}Sn from systematics. Experimental values (squares) and global BSFG predictions (triangles) for $\rho(S_n)$ are shown for various Sn isotopes as a function of S_n (see text).

for ^{122}Sn to $2.0(10) \cdot 10^5\,\mathrm{MeV}^{-1}$ [50% uncertainty assumed (see Table I)].

While we would like to normalize to $\rho(S_n)$, our experimental data only cover the excitation energy region from 0 to $S_n - 2$ MeV, due to methodical limitations. We therefore make an interpolation from our measurements to S_n using the BSFG prediction in Eq. (5). The prediction is multiplied by a scaling parameter η (see Table I) in order to agree with the normalization value $\rho(S_n)$:

$$\rho(E)_{\mathrm{BSFG}} \rightarrow \eta\,\rho(E)_{\mathrm{BSFG}}. \tag{6}$$

Figure 5 shows the normalized level densities of ^{121,122}Sn. The arrows indicate the two regions that have been used for normalization to the discrete level density and to the normalization value $\rho(S_n)$. As expected, the level-density function of ^{121}Sn is very similar to those of the other even-odd nuclei ^{117,119}Sn, while the level-density function of ^{122}Sn is very similar to those of the even-even nuclei ^{116,118}Sn [1,3].

The level densities of ^{121,122}Sn in Fig. 5 show step-like structures, a feature also seen in $^{116-119}$Sn [1,3]. In ^{121,122}Sn, two pronounced bumps are seen in the region of $\approx 0.8-1.4$ MeV and $\approx 1.8-2.4$ MeV. The corresponding steps are located at ≈ 1.0 and ≈ 2.0 MeV, respectively. The second step is very abrupt, especially in the even-even nucleus, and the step is followed by a significantly higher level density. The second step is therefore a candidate for the neutron pair-breaking process in ^{121,122}Sn. Such neutron pair-breaking bumps are especially distinctive in Sn isotopes since the proton number is magic ($Z = 50$), making proton pair breaking occur only at relatively higher excitation energies. A detailed discussion of the pair-breaking process has been given in Refs. [1,3].

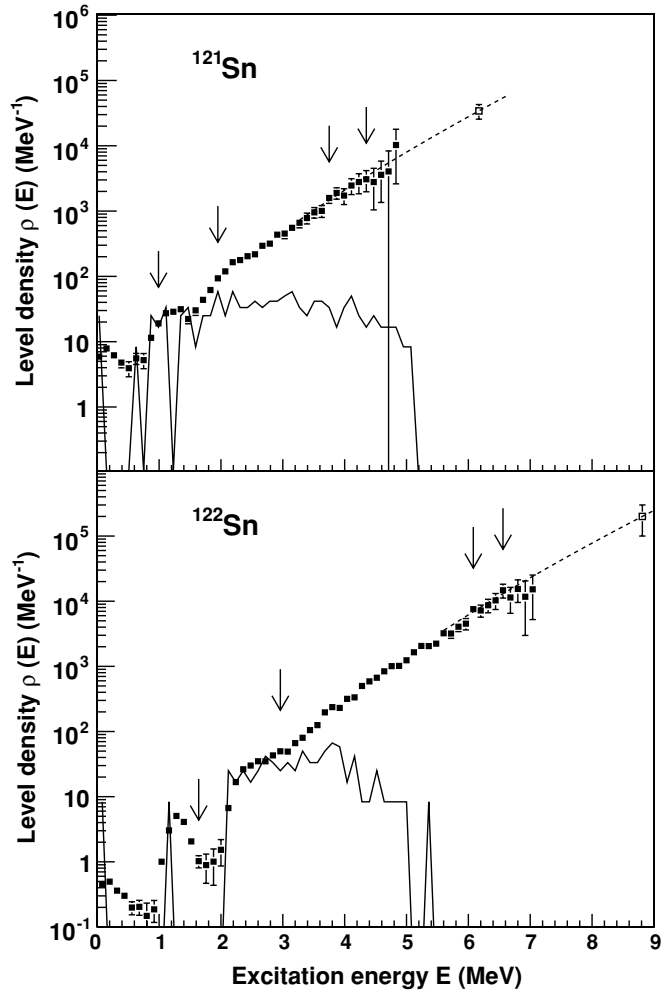

FIG. 5. Normalized level densities of ^{121,122}Sn (filled squares) as a function of excitation energy with energy bins of 120 keV/ch. The solid lines represent the discrete level densities obtained from spectroscopy. The dashed line in both panels is the BSFG prediction, which is used for interpolation, scaled with η to coincide with $\rho(S_n)$ (open square). The value of $\rho(S_n)$ has been calculated from neutron resonance data. The arrows indicate the two regions used for normalization.

V. γ-RAY STRENGTH FUNCTIONS

The γ-ray transmission coefficient $\mathcal{T}$, which is deduced from the experimental data, is related to the γ-ray strength function f by

$$\mathcal{T}(E_\gamma) = 2\pi \sum_{XL} E_\gamma^{2L+1} f_{XL}(E_\gamma), \tag{7}$$

where X denotes the electromagnetic character and L the multipolarity of the γ ray. The transmission coefficient $\mathcal{T}$ is normalized in log-scale slope (α) and in absolute value (B) [see Eq. (3)].

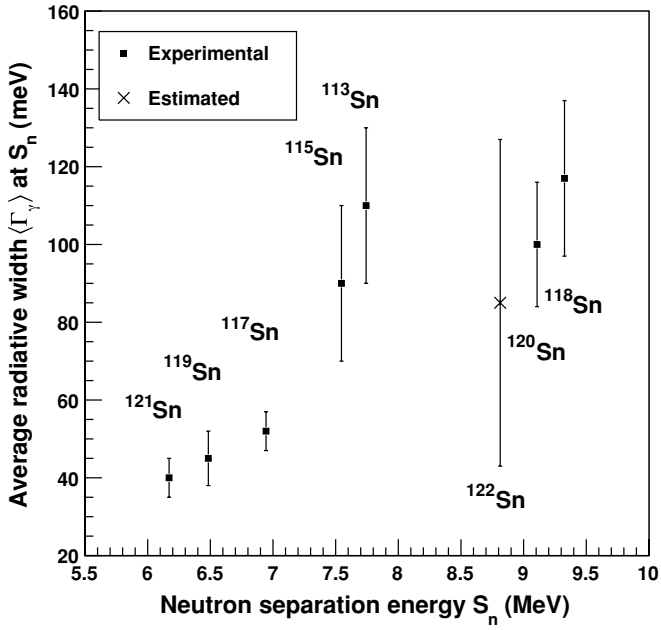

FIG. 6. Estimation of the average radiative width at S_n, $\langle\Gamma_\gamma(S_n)\rangle$, for ^{122}Sn. The respective values of other Sn isotopes are plotted (squares) as a function of S_n (see text).

For s-wave neutron resonances and assuming a major contribution from dipole radiation and parity symmetry for all excitation energies, the expression for the average radiative width $\langle\Gamma_\gamma(E, I, \pi)\rangle$ will at S_n reduce to [17]

$$\langle\Gamma_\gamma(S_n, I_t \pm 1/2, \pi_t)\rangle = \frac{B}{4\pi\ \rho(S_n, I_t \pm 1/2, \pi_t)} \int_0^{S_n} dE_\gamma\ \mathcal{T}(E_\gamma)\,\rho(S_n - E_\gamma) \times \sum_{J=-1}^{1} g(S_n - E_\gamma, I_t \pm 1/2 + J). \quad (8)$$

Here, I_t and π_t are the spin and parity of the target nucleus in the neutron capture (n,γ) reaction. We determine B by using the BSFG model for the spin distribution g given in Ref. [12] and the experimental value of $\langle\Gamma_\gamma(S_n)\rangle$.

For ^{121}Sn, the radiative width at the neutron separation energy is available in literature. For ^{122}Sn, we estimated it from systematics. Figure 6 shows the $\langle\Gamma_\gamma(S_n)\rangle$ plotted against S_n for Sn isotopes where this quantity is known (taken from Ref. [13]). From the appearing trend of the even-even nuclei, we estimate $\langle\Gamma_\gamma(S_n)\rangle$ to 85(42) meV for ^{122}Sn. The applied input parameters needed for determining the normalization constant B for ^{121,122}Sn are shown in Table II. The values for ^{121}Sn have been taken from Ref. [13].

The normalized γ-ray strength functions of ^{121,122}Sn are shown in Fig. 7. The error bars show the statistical uncertainties. While the strength function of ^{121}Sn is smooth, just like those of $^{116-119}$Sn [2,3], the strength function of ^{122}Sn displays clear structures in the entire E_γ region. As discussed in Sec. III, these structures also appear using different, independent data sets.

TABLE II. Input parameters for normalization of the γ-ray transmission coefficient $\mathcal{T}$ of ^{121,122}Sn.

Nucleus	I_t ($\hbar$)	D_0 (eV)	$\langle\Gamma_\gamma(S_n)\rangle$ (meV)
^{121}Sn	0	1250(200)	40(5)
^{122}Sn	3/2	62(31)[a]	85(42)[a]

[a]Estimated from systematics.

A change of the log-scale slope in the strength functions, leading to a sudden increase of strength, is seen in ^{121,122}Sn for $E_\gamma > 5.2$ MeV. The change of log-scale slope represents the onset of a small resonance, commonly referred to as the pygmy dipole resonance. A comparison of our ^{121,122}Sn measurements compared with photonuclear cross-section data from Refs. [18–22] is shown in the two upper panels in Fig. 8. Similar strength increases were also seen in $^{116-119}$Sn [3], and this figure will be further discussed for those isotopes when discussing the evolution of the pygmy resonance in the next section.

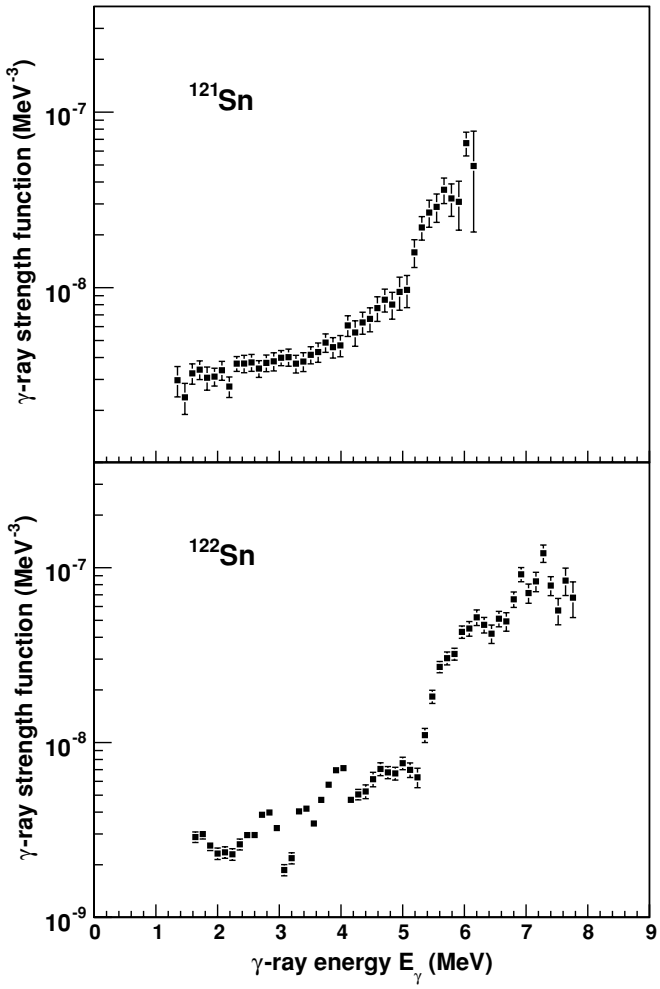

FIG. 7. Normalized γ-ray strength functions of ^{121,122}Sn as functions of γ-ray energy. The energy bins are 120 keV/ch.

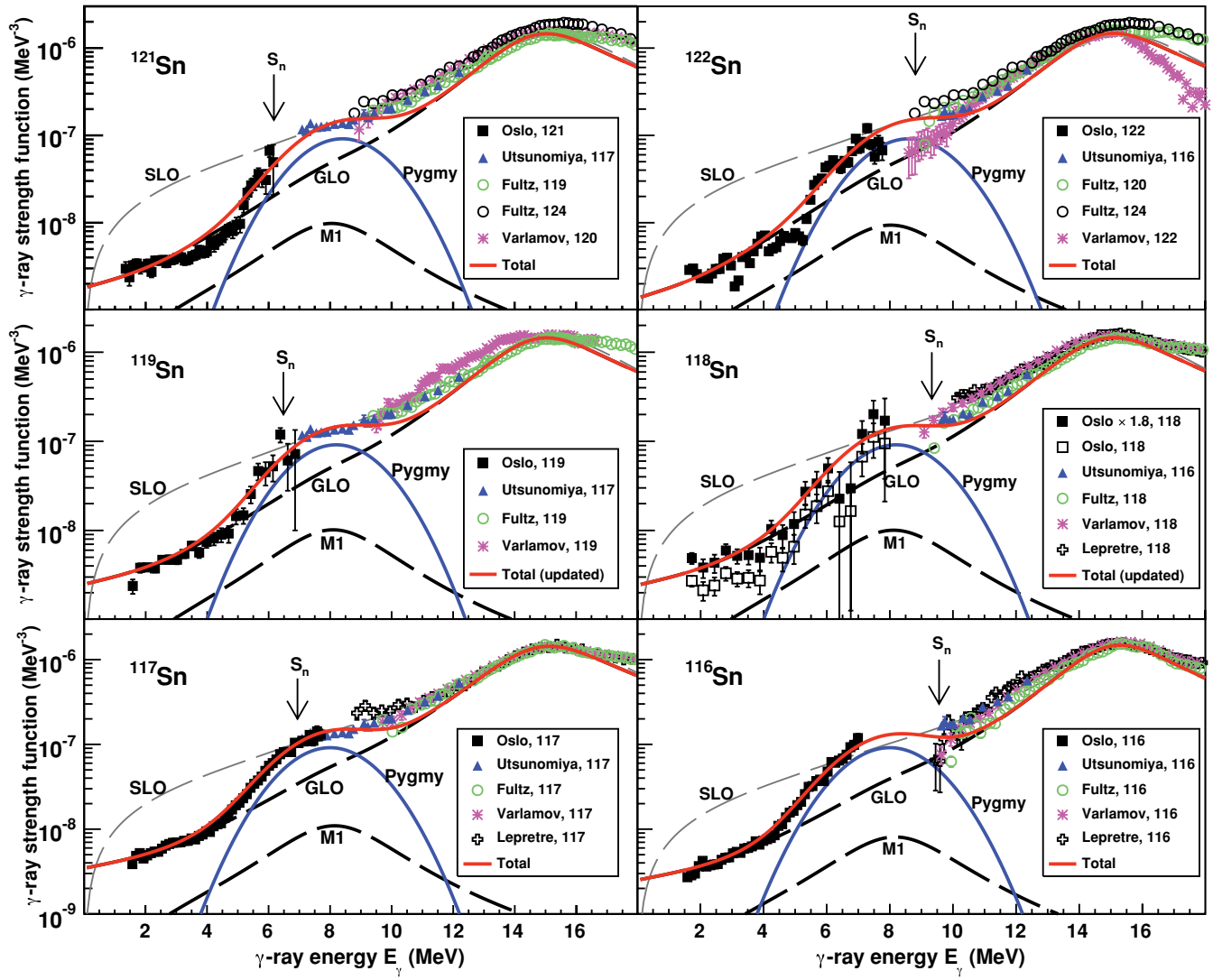

FIG. 8. (Color online) Comparison of the prediction of the total strength functions with the OCL experimental measurements for $^{116-119,121,122}$Sn. The strength function of ^{118}Sn is shown both as multiplied with 1.8 (filled squares) and as the original normalization (open squares). The arrows indicate S_n. The total strength predictions (solid lines) are modeled as Gaussian pygmy resonance additions to the GLO ($E1+M1$) baselines. The SLO ($E1+M1$) baselines are also shown. Upper left panel: ^{117}Sn(γ,n) from Utsunomiya *et al.* [19], ^{119,124}Sn(γ,x) from Fultz *et al.* [18], and ^{120}Sn(γ,x) from Varlamov *et al.* [21]. Upper right panel: ^{116}Sn(γ,n) [19], ^{120,124}Sn(γ,x) [18], and ^{122}Sn(γ,n) from Varlamov *et al.* [20]. Middle left panel: ^{117}Sn(γ,n) [19], ^{119}Sn(γ,x) [18], and ^{119}Sn(γ,n) [20]. Middle right panel: ^{116}Sn(γ,n) [19], ^{118}Sn(γ,x) [18], ^{118}Sn(γ,x) from Varlamov *et al.* [21], and ^{118}Sn(γ,x) from Leprêtre *et al.* [22]. Lower left panel: ^{117}Sn(γ,n) [19], ^{117}Sn(γ,x) [18], ^{117}Sn(γ,x) [21], and ^{117}Sn(γ,x) [22]. Lower right panel: ^{116}Sn(γ,n) [19], ^{116}Sn(γ,x) [18], ^{116}Sn(γ,x) [21], and ^{116}Sn(γ,x) [22].

In order to investigate the experimental strength functions of ^{121,122}Sn, we have applied commonly used models for the GEDR resonance and for the magnetic spin-flip resonance, also known as the giant magnetic dipole resonance (GMDR).

The generalized Lorentzian (GLO) model [23] is used for the GEDR resonance. The GLO model is known to agree rather well both for low γ-ray energies and for the GEDR centroid at about 15 MeV. The strength function approaching a nonzero value for low E_γ is not a property specific for the Sn isotopes, but has been seen for all nuclei studied at the OCL so far.

In the GLO model, the $E1$ strength function is given by [23]

$$f_{E1}^{\mathrm{GLO}}(E_\gamma) = \frac{1}{3\pi^2\hbar^2c^2}\sigma_{E1}\Gamma_{E1} \times \left[E_\gamma \frac{\Gamma_{\mathrm{KMF}}(E_\gamma, T_f)}{\left(E_\gamma^2 - E_{E1}^2\right)^2 + E_\gamma^2[\Gamma_{\mathrm{KMF}}(E_\gamma, T_f)]^2} + 0.7\,\frac{\Gamma_{\mathrm{KMF}}(E_\gamma = 0, T_f)}{E_{E1}^3} \right], \quad (9)$$

in units of MeV^{-3}, where the Lorentzian parameters are the GEDR's centroid energy E_{E1}, width Γ_{E1}, and cross section

TABLE III. Applied parameters for the parametrization of the GEDR and the GMDR contributions for ^{121,122}Sn.

Nucleus	E_{E1} (MeV)	Γ_{E1} (MeV)	σ_{E1} (mb)	E_{M1} (MeV)	Γ_{M1} (MeV)	σ_{M1} (mb)	T_f (MeV)
^{121}Sn	15.53	4.81	253.0	8.29	4.00	1.11	0.25(5)
^{122}Sn	15.59	4.77	256.0	8.27	4.00	1.09	0.25(5)

σ_{E1}. These experimental parameters are not available for ^{121,122}Sn. We instead apply the one measured for ^{120}Sn to ^{121}Sn, and the one measured for ^{124}Sn to ^{122}Sn, from Fultz [18] (see Table III).

The GLO model is temperature dependent from the incorporation of a temperature-dependent width $\Gamma_{\rm KMF}$. This width is the term responsible for the nonvanishing $E1$ strength at low excitation energy. It has been adopted from the Kadmenskič, Markushev, and Furman (KMF) model [24] and is given by

$$\Gamma_{\rm KMF}(E_\gamma, T_f) = \frac{\Gamma_r}{E_r^2}\left(E_\gamma^2 + 4\pi^2 T_f^2\right), \qquad (10)$$

in units of MeV, and where T_f is the temperature.

Usually, T_f is interpreted as the nuclear temperature of the final state, with the commonly applied expression $T_f = \sqrt{U/a}$. In this work and in Refs. [1–3], we assume a constant temperature, i.e., the γ-ray strength function is independent of excitation energy. This approach is adopted for consistency with the Brink-Axel hypothesis (see Sec. III).

Moreover, we treat T_f as a free parameter. This is necessary to adjust the theoretical strength prediction to our low-energy measurements. The applied values of the T_f parameters are listed in Table III.

The $M1$ spin-flip resonance is modeled with the functional form of a standard Lorentzian (SLO) model [25]:

$$f_{M1}^{\rm SLO}(E_\gamma) = \frac{1}{3\pi^2\hbar^2c^2}\frac{\sigma_{M1}\Gamma_{M1}^2 E_\gamma}{\left(E_\gamma^2 - E_{M1}^2\right)^2 + E_\gamma^2\,\Gamma_{M1}^2}, \qquad (11)$$

where the parameter E_{M1} is the centroid energy, Γ_{M1} is the width, and σ_{M1} is the cross section of the GMDR. These Lorentzian parameters are for ^{121,122}Sn predicted from the theoretical expressions in Ref. [25] and shown in Table III. The predictions for the GEDR using the GLO model and for the GMDR for $^{116-119,121,122}$Sn nuclei are shown as dashed lines in Fig. 8.

The standard Lorentzian (SLO) model was also tested and is included in Fig. 8 (the $M1$ spin-flip resonance contribution is added to it). The SLO succeeds in reproducing the (γ, x) data, but clearly fails for the low-energy strength measurements, both when it comes to absolute value and shape. The same has been the case also for many other nuclei measured at the OCL and elsewhere. Therefore, we consider the SLO not to be adequate below the neutron threshold.

At present, it is unclear how these resonances should be modeled properly, although many theoretical predictions exist. We have found [2,3] that the Sn pygmy resonance is satisfactorily reproduced by a Gaussian distribution [2]:

$$f_{\rm pyg}(E_\gamma) = C_{\rm pyg}\frac{1}{\sqrt{2\pi}\,\sigma_{\rm pyg}}\exp\left[\frac{-(E_\gamma - E_{\rm pyg})^2}{2\sigma_{\rm pyg}^2}\right], \qquad (12)$$

superimposed on the GLO prediction. Here, $C_{\rm pyg}$ is the resonance's absolute value normalization constant, $E_{\rm pyg}$ is the centroid energy, and $\sigma_{\rm pyg}$ is the width. These parameters are treated as free.

TABLE IV. Empirical values of Gaussian pygmy parameters, and the corresponding integrated strengths and TRK values of the pygmy resonances, in ^{121,122}Sn.

Nucleus	$E_{\rm pyg}$ (MeV)	$\sigma_{\rm pyg}$ (MeV)	$C_{\rm pyg}$ (10^{-7} MeV^{-2})	Integrated strength (MeV mb)	TRK value (%)
^{121}Sn	8.4(1)	1.4(1)	3.2^{+3}_{-9}	31^{+3}_{-8}	1.8^{+1}_{-5}
^{122}Sn	8.6(2)	1.4(1)	3.2^{+3}_{-9}	32^{+2}_{-9}	1.8^{+1}_{-5}

By adding the discussed theoretical strength contributions, the prediction of the total γ-ray strength function is given by

$$f_{\rm total} = f_{E1} + f_{M1} + f_{\rm pyg}\,. \qquad (13)$$

We determined the Gaussian pygmy parameters of ^{121,122}Sn from fitting to our measurements. The centroid energies of the pygmy resonances are 8.4(1) and 8.6(2) MeV, respectively. We found that the same width $\sigma_{\rm pyg}$ and strength $C_{\rm pyg}$ as in ^{116,117}Sn [3] gave a very good agreement also in ^{121,122}Sn, so the width and strength are kept unchanged. The pygmy parameters are listed in Table IV. The estimated error bars given in the table take into account systematic uncertainties in the normalization values and in the choice of baseline of the pygmy resonance, including the fact that the GLO does not perfectly follow the (γ, n) measurements for higher E_γ values.

The predictions for ^{121,122}Sn are shown as solid lines in the upper panels of Fig. 8. We see that the predictions of the total strength describe the measurements rather well, in the sense that the Gaussian pygmy resonances fill a very large fraction of the missing strength. Still, the Gaussian distribution does not completely follow either the left flank or the right flank of the pygmy resonances in ^{121,122}Sn. In the case of ^{116,117}Sn [2,3], having a larger T_f of $T_f = 0.46(1)$ MeV, the left flank was followed very well. However, in all Sn isotopes, there is a gap on the right flank between the measured data and the GLO. A better pygmy resonance representation than the Gaussian or a better model for the baseline may be found in the future.

Strength from the resonances in ^{121,122}Sn have been added in the energy region of $\approx$5–8 MeV according to our measurements, and in the region of $\approx$5–11 MeV when compared to photonuclear data as well. The total integrated strengths of the pygmy resonances, based on the total predictions, are estimated to 32^{+3}_{-9} MeV mb. This constitutes 1.8^{+1}_{-5}% of the classical Thomas-Reiche-Kuhn (TRK) sum rule, assuming all pygmy resonance strength being $E1$ (see Table IV).

Even though uncertainties in the choice of baseline have been considered in the uncertainty estimates, another prediction of the GEDR other than the GLO or another function for the pygmy resonance than the Gaussian may be found in

the future. This will consequently influence the estimates on the pygmy resonance. Lack of data, i.e., the gaps between our measurements and the (γ,n) measurements in the resonance region, and also the lack of (γ,n) measurements for ^{121,122}Sn, adds to the uncertainties in the estimates of the pygmy resonances.

Measurements from other reactions and using other methods have also been used to estimate the TRK value of the Sn pygmy, and these estimates deviate from each other. Data from ^{116,117}Sn(γ,n) experiments [19] indicate an integrated strength which constitutes $\approx$1% of the TRK sum rule, which agrees within the uncertainty with our value. From ^{116,124}Sn(γ,γ') experiments [26], the TRK value is calculated to 0.4−0.6 %. This may seem to deviate from our result. However, taking into account unresolved strength in the quasicontinuum of typically a factor of 2−3, the (γ,γ') results are compatible within the uncertainty with the other data.

VI. EVOLUTION OF THE PYGMY RESONANCE

Studying the neutron dependency is important and may help in determining the origin of the Sn pygmy resonance. Figure 9 shows the present and previously analyzed normalized strength functions for the Sn isotopes. The measurements of ^{118}Sn have been multiplied by 1.8 in order to agree with those of ^{116}Sn (see Ref. [3]).

First, it may seem like a trend that the tail of the strength function decreases in strength as the neutron number N increases. Second, it is noticeable from Fig. 9 that the change of log-scale slope, which represents the onset of the pygmy resonance, occurs at a higher E_γ value in ^{121,122}Sn than for ^{116,117}Sn. The changes of slope are clearest for the even-even nuclei. They are found at $\approx$4.5 MeV in ^{116}Sn and at $\approx$5.2 MeV in ^{122}Sn.

The values of T_f for ^{121,122}Sn are lower than for $^{116-119}$Sn. There is no physical reason for different nuclear temperatures. Lowering the parameter T_f is instead necessary in order to get the lowest-energy part of the GLO comparable in magnitude with the measurements.

The centroid energy $E_{\rm pyg}$ of the pygmy resonances in ^{121,122}Sn has larger values than those of earlier studies in ^{116,117}Sn [2,3]. For ^{121,122}Sn, the pygmy centroids are 8.4(1) and 8.6(2) MeV (see Table IV), respectively, while 8.0(1) MeV is found for ^{116,117}Sn [2,3]. During the pygmy resonance fitting, it was clear that the centroid energies had to be significantly increased for the heavier isotopes. The significant increases are also apparent from studying the energies for which there is a change of log-scale slope in the strength functions. Moreover, allowing the centroid energy differ has a consequence that the same pygmy width $\sigma_{\rm pyg}$ and pygmy strength $C_{\rm pyg}$ as in ^{116,117}Sn [3] also give the best fit in ^{121,122}Sn.

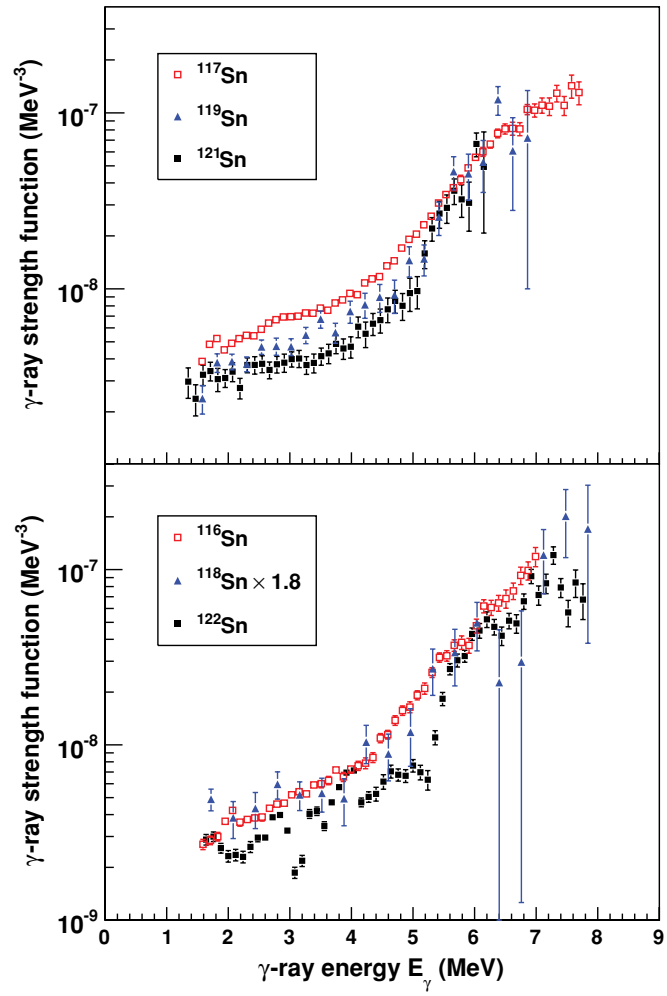

FIG. 9. (Color online) Normalized γ-ray strength functions as functions of γ-ray energy for the Sn isotopes measured at the OCL. The even-odd isotopes ^{117,119,121}Sn are shown in the upper panel, while the even-even isotopes ^{116,118,122}Sn are shown in the lower panel. The measured strength of ^{118}Sn has been multiplied by 1.8 (see Ref. [3]). The energy bins are 120 keV/ch for ^{116,117,121,122}Sn, 240 keV/ch for ^{119}Sn, and 360 keV/ch for ^{118}Sn.

TABLE V. Empirical values of $^{116-119}$Sn Gaussian pygmy parameters, and the corresponding pygmies' integrated strengths and TRK values. For ^{118}Sn, the values have been found from fitting to the measured strength function multiplied by 1.8.

Nucleus	$E_{\rm pyg}$ (MeV)	$\sigma_{\rm pyg}$ (MeV)	$C_{\rm pyg}$ (10^{-7} MeV^{-2})	Integrated strength (MeV mb)	TRK value (%)
^{116}Sn	8.0(1)	1.4(1)	3.2^{+3}_{-9}	30^{+0}_{-8}	1.7^{+0}_{-4}
^{117}Sn	8.0(1)	1.4(1)	3.2^{+3}_{-9}	30^{+0}_{-8}	1.7^{+0}_{-4}
^{118}Sn	8.2(1)	1.4(1)	3.2^{+0}_{-9}	30^{+0}_{-8}	1.8^{+0}_{-5}
^{119}Sn	8.2(1)	1.4(1)	3.2^{+0}_{-9}	30^{+0}_{-8}	1.7^{+0}_{-4}

TABLE VI. Applied parameters for the parametrization of the GEDR and the GMDR contributions for $^{116-119}$Sn.

Nucleus	E_{E1} (MeV)	Γ_{E1} (MeV)	σ_{E1} (mb)	E_{M1} (MeV)	Γ_{M1} (MeV)	σ_{M1} (mb)	T_f (MeV)
^{116}Sn	15.68	4.19	266.0	8.41	4.00	0.773	0.46(1)
^{117}Sn	15.66	5.02	254.0	8.38	4.00	1.04	0.46(1)
^{118}Sn	15.59	4.77	256.0	8.36	4.00	0.956	0.40(1)
^{119}Sn	15.53	4.81	253.0	8.34	4.00	0.963	0.40(1)

In the earlier study of ^{118,119}Sn [3], the data have large error bars. This means that the pattern of an increasing centroid energy was not so clear, and the choice then was to keep the centroid energy constant, while compensating with an increase of the resonance width. We have updated the resonance prediction of ^{118,119}Sn by following the same pattern as in ^{121,122}Sn. The estimated centroid energy of the pygmies in ^{118,119}Sn is then 8.2(1) MeV, while the width and strength are kept constant. Updated parameter values are listed in Table V and displayed in Fig. 8. The parameters for the GEDR and GMDR contributions are listed in Table VI.

We would like to investigate for several isotopes the effect of our predicted pygmy resonances on the (n,γ) cross sections and compare these with available experimental measurements. This has been done for $^{117-119,121}$Sn using the reaction code TALYS [27]. For the level density, we have applied the spin- and parity-dependent calculations of Goriely, Hilaire, and Koning [28], which are in good agreement with our level-density data, as demonstrated for ^{117}Sn in Fig. 10. Also, we have used the neutron optical potential of Koning and Delaroche [29].

The results of the comparisons are shown in Fig. 11. Our modeled strength function with a Gaussian pygmy resonance (denoted GLO2) leads to a calculated cross section that

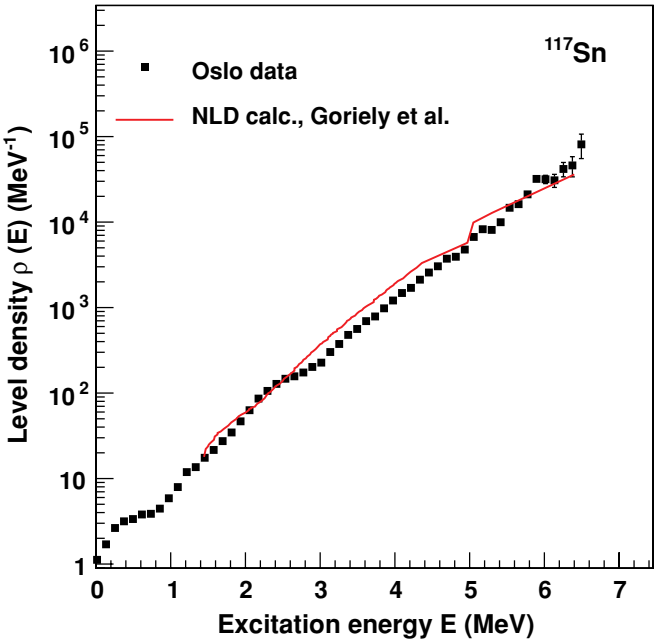

FIG. 10. (Color online) Level-density measurements on ^{117}Sn compared with microscopic calculations from Ref. [28].

generally agrees very well with the measurements. Assuming the GLO model with constant temperature but without the pygmy resonance (GLO1), clearly gives a lower cross section in all cases, as expected. This may be taken as support of the finding of an enhanced strength function in the E_γ region of $\approx$5−11 MeV. The SLO model gives an overall too high cross section, which is not surprising considering the large overshoot in γ-ray strength compared to our measurements and also to $\langle\Gamma_\gamma\rangle$ data. We note that our calculated cross section for ^{116}Sn$(n,\gamma)^{117}$Sn using the GLO2 model is in very good agreement with the one in the work of Utsunomiya *et al.* [19].

For the ^{117}Sn$(n,\gamma)^{118}$Sn case, we have applied the model parameters that correspond to our scaled data (with a factor of 1.8). The resulting excellent agreement with the experimental (n,γ) data further supports our choice of renormalization in Ref. [3]. In addition, we have tested the strength prediction using parameters that fit with the original normalization, which results in calculated cross sections that are clearly underpredictive compared to the experimental data (not shown here).

The reproduction of the ^{120}Sn$(n,\gamma)^{121}$Sn cross section is not as good as for the other nuclei, as this calculation seems to be somewhat more underpredictive. However, the calculation is certainly an improvement compared to that of the GLO1, which is a standard strength model without the pygmy resonance. The underprediction might be explained by a too low experimental value of $\langle\Gamma_\gamma\rangle$ in the normalization procedure of the measurements. If the value had been higher, the pygmy resonance would have produced more strength, leading to a general increase of the calculated cross section.

We would also like to study the evolution of the resonances' centroid energy $E_{\rm pyg}$ with neutron number N. Figure 12 shows $E_{\rm pyg}$ as a function of N for the isotopes studied at the OCL. A χ^2 fit has been performed on these data, resulting in the linear relation $E_{\rm pyg} = 2.0(16) + 0.090(23)N$ in units of MeV.

The estimates on $E_{\rm pyg}$ from others' experimental data on Sn are in agreement within the uncertainties with the observed pattern: $\approx$8.5 MeV for ^{116,117}Sn [19], $\approx$7.8 MeV for ^{117,119}Sn [35], and 10.1(7) and 9.8(7) MeV for ^{130,132}Sn [36], respectively. Note that an increase of the resonances' centroid energies with increasing neutron numbers was also found in experimental data on Ca [37].

The observation of an increase of the centroid energy with increasing neutron numbers is not in agreement with common theoretical predictions. On the contrary, studies on Sn isotopes instead predict a decrease of centroid energy with increasing neutron numbers. These studies include the Hartree-Fock-Bogoljubov (HFB) and multiphonon quasiparticle-phonon models (QPM) by Tsoneva and Lenske [38], the relativistic Hartree-Bogoliubov model (RHB) + relativistic quasiparticle random phase approximation (RQRPA) (DD-ME2) model by Paar [39], and the continuum QRPA model by Daoutidis [40]. Also, a theoretical study on Ca isotopes, using the extended theory of finite Fermi systems (ETFFS) by Tertychny [37], results in a decrease of centroid energy with neutron number (contrary to experimental results on Ca, see Ref. [37], and references therein). However, it is noted that Daoutidis [40]

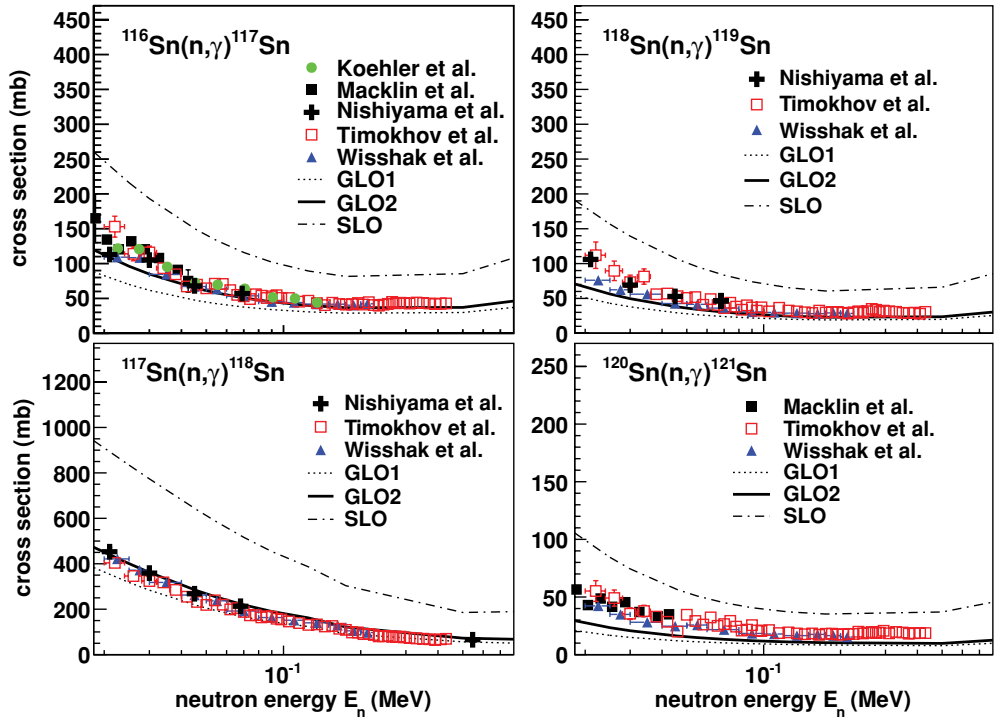

FIG. 11. (Color online) Data on neutron-capture cross sections for the target nuclei $^{116-118,120}$Sn compared with calculations for neutron energies $\gtrsim$20 keV. GLO1 (dotted line) is the GLO model assuming constant temperatures (given in Tables IV and VI) and GLO2 (solid line) is the GLO1 model plus the prediction of the pygmy resonance. Measurements are from Koehler *et al.* [30], Macklin *et al.* [31], Nishiyama *et al.* [32], Wisshak *et al.* [33], and Timokhov *et al.* [34].

predicts a relatively stable centroid energy in the atomic mass region $A = 120-126$ compared to other mass regions. Hence, the increase of centroid energy in the isotopes that we have compared may be less than would have been observed in another mass region.

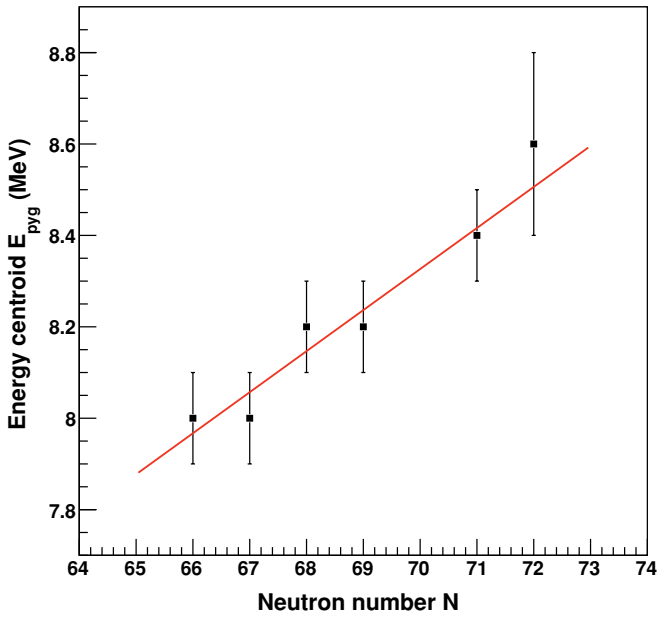

FIG. 12. (Color online) Estimated centroid energies E_{pyg} (squares) as a function of neutron number N, deduced from our measurements on $^{116-119,121,122}$Sn. The solid line is a linear χ^2 fit to the measurements.

Recent measurements using the $(\alpha, \alpha'\gamma)$ coincidence method on ^{124}Sn compared to photon-scattering experiments show a splitting into its isoscalar and isovector components [41]. Hence, both components seem to be present, in agreement with theoretical predictions.

The nature, origin, and integrated strength of the Sn pygmy resonance are issues that are heavily debated. The $E1$ neutron-skin oscillation mode, discussed in Refs. [39,42,43], is assumed as the underlying physical phenomenon in most of the theoretical predictions, both in macroscopic (e.g., Van Isacker *et al.* [42]) and microscopic approaches (e.g., Daoutidis [40], Tsoneva and Lenske [38], Paar [39], and Sarchi *et al.* [43]). Most theoretical calculations predict a systematic increase of the resonances' strength as the number of neutrons increase, due to the increase of the number of neutrons in the skin. Another prediction is the increase by neutron number up to ^{120}Sn followed by a decrease (Paar [39]). Several of the predicted increases of integrated strength concerning the isotopes that we have performed measurements on are significant (e.g., Tsoneva and Lenske [38], Van Isacker *et al.* [42], and Litvinova *et al.* [44]). It is noted that the study by Daoutidis [40] predicts that also the integrated strength is relatively stable in the mass region $A = 120-126$.

However, for our measurements on the pygmy resonances in $^{116-119,121,122}$Sn, we cannot see any dependency on neutron number in the integrated strengths. The same resonance prediction has, on the contrary, been applied for all isotopes.

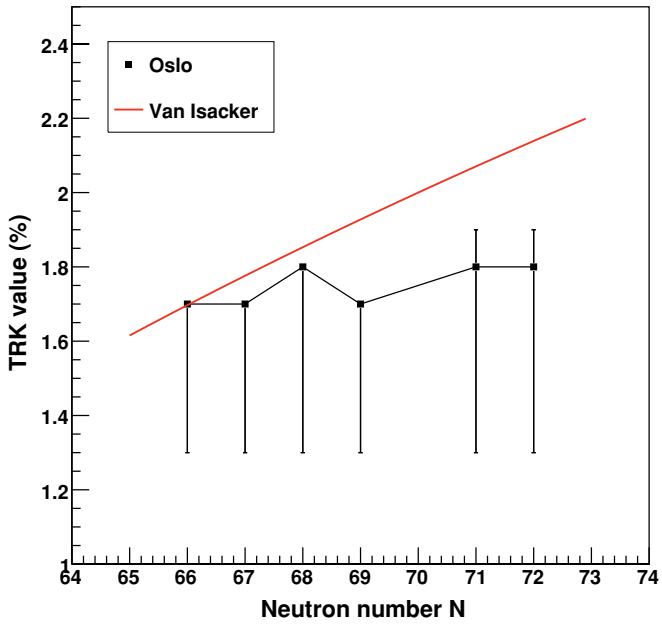

FIG. 13. (Color online) TRK values for Sn estimated from our measurements (squares) compared to the theoretical prediction from Van Isacker *et al.* [42] (multiplied by a factor 14) (solid line) as a function of neutron number N.

[The total integrated strengths and the TRK values of ^{121,122}Sn being slightly larger than those of ^{116,117}Sn (see Tables IV and V) is explained by differences in the GLO models of those isotopes.] Figure 13 shows our TRK values together with those of Van Isacker *et al.* [42] (multiplied by a factor of 14 in absolute value). The experimental result does not follow the predicted increase. Still, the uncertainties in our estimated resonance strengths are large. More experimental information is therefore needed in order to answer the question of whether the integrated strength in Sn increases with neutron number.

The experimental TRK values based on ours and others' measurements are relatively large, compared to general excitations. This might indicate that the pygmy resonance is due to a collective phenomenon. However, its origin is unknown, and single-particle excitations are not excluded. Various theoretical predictions disagree on whether the neutron-skin oscillation is collective or not [39].

A clarification of the electromagnetic character of the pygmy resonance in Sn would be of utmost importance. Present theoretical predictions assume an $E1$ strength, modeling the resonance as a neutron-skin oscillation. Experimental studies have indicated an $E1$ character. Amongst these are the nuclear resonance fluorescence (NRF) experiments performed on ^{116,124}Sn [26] and ^{112,124}Sn [45], and the Coulomb dissociation experiments performed on $^{129-132}$Sn [36,46]. In addition are the polarized photon beam experiments on ^{138}Ba [47]. However, the existence of an $M1$ component of the resonance strength cannot be ruled out, as was discussed in Ref. [3].

VII. CONCLUSIONS

The level density and γ-ray strength functions of ^{121,122}Sn have been measured using the (^{3}He,^{3}He$'\gamma$) and (^{3}He,$\alpha\gamma$) reactions and the Oslo method. The level densities of ^{121,122}Sn display steplike structures for excitation energies below $\approx$4 MeV. One of the bumps is interpreted as a signature of neutron pair breaking, in accordance with the findings in $^{116-119}$Sn.

A significant enhancement in the γ-ray strength is observed in the ^{121,122}Sn measurements for $E_\gamma \gtrsim 5.2$ MeV. The integrated strength of the resonances correspond to $\approx 1.8^{+1}_{-5}\%$ of the TRK sum rule. These enhancements are compatible with pygmy resonances centered at $\approx$8.4(1) and $\approx$8.6(2) MeV, respectively.

Neutron-capture cross-section calculations using our pygmy resonance predictions give significantly better reproduction of experimental (n,γ) cross sections than standard strength models without any pygmy resonance.

The pygmy resonances are compared to those observed in $^{116-119}$Sn. The evolution with increasing neutron numbers of the pygmy resonances observed in $^{116-119,121,122}$Sn is a clear increase of centroid energy from 8.0(1) MeV in ^{116}Sn to 8.6(2) MeV in ^{122}Sn, while no difference in integrated strength is observed. This finding is not in agreement with most theoretical predictions. However, the experimental uncertainties are large, and more experimental information is needed in order to determine the nature of the pygmy resonances in the Sn isotopes.

ACKNOWLEDGMENTS

We would like to thank H. Utsunomiya for giving us access to yet unpublished experimental results from photoneutron cross-section reactions ^{120,122}Sn(γ,n), and the Department of Physics at the University of Jyväskylä (JYFL) for kindly lending us the ^{122}Sn target. We also thank E. A. Olsen, J. Wikne, and A. Semchenkov for excellent experimental conditions. The funding of this research from The Research Council of Norway (Norges forskningsråd) is gratefully acknowledged.

[1] U. Agvaanluvsan, A. C. Larsen, M. Guttormsen, R. Chankova, G. E. Mitchell, A. Schiller, S. Siem, and A. Voinov, Phys. Rev. C **79**, 014320 (2009).
[2] U. Agvaanluvsan, A. C. Larsen, R. Chankova, M. Guttormsen, G. E. Mitchell, A. Schiller, S. Siem, and A. Voinov, Phys. Rev. Lett. **102**, 162504 (2009).
[3] H. K. Toft *et al.*, Phys. Rev. C **81**, 064311 (2010).
[4] M. Guttormsen, A. Atac, G. Løvhøiden, S. Messelt, T. Ramsøy, J. Rekstad, T. F. Thorsteinsen, T. S. Tveter, and Z. Zelazny, Phys. Scr., T **32**, 54 (1990).
[5] M. Guttormsen, T. S. Tveter, L. Bergholt, F. Ingebretsen, and J. Rekstad, Nucl. Instrum. Methods Phys. Res. A **374**, 371 (1996).
[6] M. Guttormsen, T. Ramsøy, and J. Rekstad, Nucl. Instrum. Methods Phys. Res. A **255**, 518 (1987).
[7] A. C. Larsen *et al.*, Phys. Rev. C **83**, 034315 (2011).
[8] A. Schiller, L. Bergholt, M. Guttormsen, E. Melby, J. Rekstad, and S. Siem, Nucl. Instrum. Methods Phys. Res. A **447**, 498 (2000).

[9] A. Bohr and B. Mottelson, *Nuclear Structure* (Benjamin, New York, 1969), Vol. I.
[10] D. M. Brink, Ph.D. thesis, Oxford University, 1955.
[11] P. Axel, Phys. Rev. **126**, 671 (1962).
[12] T. von Egidy, H. H. Schmidt, and A. N. Behkami, Nucl. Phys. A **481**, 189 (1988).
[13] R. Capote *et al.*, Nucl. Data Sheets **110**, 3107 (2009). Available online at [http://www-nds.iaea.org/RIPL-3/].
[14] G. Audi and A. H. Wapstra, Nucl. Phys. A **595**, 409 (1995).
[15] J. Dobaczewski, P. Magierski, W. Nazarewicz, W. Satuła, and Z. Szymański, Phys. Rev. C **63**, 024308 (2001).
[16] A. Gilbert and A. G. W. Cameron, Can. J. Phys. **43**, 1446 (1965).
[17] A. Voinov, M. Guttormsen, E. Melby, J. Rekstad, A. Schiller, and S. Siem, Phys. Rev. C **63**, 044313 (2001).
[18] S. C. Fultz, B. L. Berman, J. T. Caldwell, R. L. Bramblett, and M. A. Kelly, Phys. Rev. **186**, 1255 (1969).
[19] H. Utsunomiya *et al.*, Phys. Rev. C **80**, 055806 (2009).
[20] V. V. Varlamov, B. S. Ishkhanov, V. N. Orlin, and V. A. Tchetvertkova, Moscow State University Institute of Nuclear Physics Report No. 2009, p. 3/847 (2009).
[21] V. V. Varlamov, N. N. Peskov, D. S. Rudenko, and M. E. Stepanov, Vop. At. Nauki i Tekhn., Ser. Yadernye Konstanty 1-2 (2003).
[22] A. Leprêtre, H. Beil, R. Bergere, P. Carlos, A. De Miniac, A. Veyssiere, and K. Kernbach, Nucl. Phys. A **219**, 39 (1974).
[23] J. Kopecky and R. E. Chrien, Nucl. Phys. A **468**, 285 (1987).
[24] S. G. Kadmenskii, V. P. Markushev, and V. I. Furman, Yad. Fiz. **37**, 277 (1983) [Sov. J. Nucl Phys. **37**, 165 (1983)].
[25] T. Belgya *et al.*, *Handbook for Calculations of Nuclear Reaction Data*, *RIPL-2*, (IAEA, Vienna, 2006). Available online at [http://www-nds.iaea.org/RIPL-2/].
[26] K. Govaert, F. Bauwens, J. Bryssinck, D. De Frenne, E. Jacobs, W. Mondelaers, L. Govor, and V. Y. Ponomarev, Phys. Rev. C **57**, 2229 (1998).
[27] A. J. Koning, S. Hilaire, and M. C. Duijvestijn, in *"TALYS-1.2," Proceedings of the International Conference on Nuclear Data for Science and Technology, Nice, France, 2007,* edited by O. Bersillon, F. Gunsing, E. Bauge, R. Jacqmin, and S. Leray (EDP Sciences, 2008), p. 211. Available online at [http://www.talys.eu/].
[28] S. Goriely, S. Hilaire, and A. J. Koning, Phys. Rev. C **78**, 064307 (2008).
[29] A. J. Koning and J. P. Delaroche, Nucl. Phys. A **713**, 231 (2003).
[30] P. E. Koehler, R. R. Spencer, K. H. Guber, J. A. Harvey, N. W. Hill, and R. R. Winters, in *Proceedings of the International Conference on Nuclear Data for Science and Technology*, *Trieste, Italy, 1997*, edited by G. Reffo, A. Ventura, and G. Grandi (Italian Physical Society, Bologna, Italy, 1997).
[31] R. L. Macklin, T. Inada, and J. H. Gibbons, Nature (London) **194**, 1272 (1962).
[32] J. Nishiyama, M. Igashira, T. Ohsaki, G. N. Kim, W. C. Chung, and T. I. Ro, J. Nucl. Sci. Technol. (Tokyo) , **45**, 352 (2008).
[33] K. Wisshak, F. Voss, Ch. Theis, F. Käppeler, K. Guber, L. Kazakov, N. Kornilov, and G. Reffo, Phys. Rev. C **54**, 1451 (1996).
[34] V. M. Timokhov, M. V. Bokhovko, M. V. Isakov, L. E. Kazakov, V. N. Kononov, G. N. Manturov, E. D. Poletaev, and V. G. Pronyaev, Yad. Fiz. **50**, 609 (1989).
[35] E. J. Winhold, E. M. Bowey, D. B. Gayther, and B. H. Patrick, Phys. Lett. **32B**, 7 (1970).
[36] P. Adrich *et al.*, Phys. Rev. Lett. **95**, 132501 (2005).
[37] G. Tertychny, V. Tselyaev, S. Kamerdzhiev, F. Grümmer, S. Krewald, J. Speth, A. Avdeenkov, and E. Litvinova, Phys. Lett. B **647**, 104 (2007).
[38] N. Tsoneva and H. Lenske, Phys. Rev. C **77**, 024321 (2008).
[39] N. Paar, Rep. Prog. Phys. **70**, 691 (2007).
[40] I. Daoutidis (private communication).
[41] J. Endres *et al.*, Phys. Rev. Lett. **105**, 212503 (2010).
[42] P. Van Isacker, M. A. Nagarajan, and D. D. Warner, Phys. Rev. C **45**, R13 (1992).
[43] D. Sarchi, P. F. Bortignon, and G. Colo, Phys. Lett. B **601**, 27 (2004).
[44] E. Litvinova, P. Ring, and V. Tselyaev, Phys. Rev. Lett. **105**, 022502 (2010).
[45] A. Tonchev (private communication).
[46] Klimkiewicz *et al.*, Phys. Rev. C **76**, 051603(R) (2007).
[47] A. Tonchev *et al.*, Phys. Rev. Lett. **104**, 072501 (2010).